

Article

# Pore Formation Mechanism of A-Beta Peptide on the Fluid Membrane: A Combined Coarse-Grained and All-Atomic Model

Yuxi Dai <sup>1</sup>, Zhexing Xie <sup>2</sup> and Lijun Liang <sup>1,\*</sup><sup>1</sup> College of Automation, Hangzhou Dianzi University, Hangzhou 310018, China; 20068815@hdu.edu.cn<sup>2</sup> College of Accounting, Hangzhou Dianzi University, Hangzhou 310018, China; 20140935@hdu.edu.cn

\* Correspondence: llj@hdu.edu.cn

**Abstract:** In Alzheimer's disease, ion permeability through the ionic channel formed by A $\beta$  peptides on cellular membranes appears to underlie neuronal cell death. An understanding of the formation mechanism of the toxic ionic channel by A $\beta$  peptides is very important, but remains unclear. Our simulation results demonstrated the dynamics and mechanism of channel formation by A $\beta$ 1-28 peptides on the DPPC and POPC membrane by the coarse-grained method. The ionic channel formation is driven by the gyration of the radius and solvent accessible molecular surface area of A $\beta$ 1-28 peptides. The ionic channel formation mechanism was explored by the free energy profile based on the distribution of the gyration of the radius and solvent accessible molecular surface area of A $\beta$ 1-28 peptides on the fluid membrane. The stability and water permeability of the ionic channel formed by A $\beta$  peptides was investigated by all-atomic model simulation. Our simulation showed that the ionic channel formed by A $\beta$ 1-28 peptides is very stable and has a good water permeability. This could help us to understand the pore formation mechanism by A $\beta$ 1-28 peptides on the fluidic membrane. It also provides us with a guideline by which to understand the toxicity of A $\beta$ 1-28 peptides' pores to the cell.



**Citation:** Dai, Y.; Xie, Z.; Liang, L. Pore Formation Mechanism of A-Beta Peptide on the Fluid Membrane: A Combined Coarse-Grained and All-Atomic Model. *Molecules* **2022**, *27*, 3924. <https://doi.org/10.3390/molecules27123924>

Academic Editor: Fernando Albericio

Received: 6 May 2022

Accepted: 13 June 2022

Published: 18 June 2022

**Publisher's Note:** MDPI stays neutral with regard to jurisdictional claims in published maps and institutional affiliations.



**Copyright:** © 2022 by the authors. Licensee MDPI, Basel, Switzerland. This article is an open access article distributed under the terms and conditions of the Creative Commons Attribution (CC BY) license (<https://creativecommons.org/licenses/by/4.0/>).

**Keywords:** pore formation; multiscale modeling; Alzheimer's disease; ionic channel

## 1. Introduction

Alzheimer's disease (AD) is a progressive, irreversible neurological disease [1–3]. It is the result of protein misfolding which transforms the three-dimensional conformations from native to nonnative (insoluble) folded structures [4–6]. One increasingly accepted hypothesis is that oligomer amyloid seeds are the toxic species [7–10]. The mechanism of toxicity involves the penetration of small oligomers into the membrane and formation of unregulated ion channels, which lead to ion leakage and, ultimately, cell death [11–15]. Scala et al. found that calcium could pretreat through the pore formed by beta-amyloid peptide [16]. However, the hypothesis of an ionic channel formed from A $\beta$  peptides is still under the debated. In addition, given their dynamic nature, the experimental structures for these channels are still very difficult to obtain [17,18]. Standard tools of structural biology have failed to provide the high-resolution 3D structures of the oligomers of the A $\beta$  peptide, especially on the membrane. Only low-resolution structural data from circular dichroism, electron microscopy and atomic force microscopy measurements are available [19–21]. In the groundbreaking 2020 study by Natàlia Carulla and coworkers, the first atomic structures of A $\beta$ (1–42) oligomers were resolved [22]. These elegant findings indicate that membrane-embedded A $\beta$ (1–42) oligomers form edge-conductivity pores [22]. However, a comprehensive understanding of the ion channels formed by A $\beta$  peptides is still unclear, and thus, these need to be explored.

To understand the formed ionic channel in much greater depth, theoretical calculations, especially molecular dynamics (MD) simulations, have been used to explore the A-beta

aggregation process [23–27]. Nussinov and his coworkers designed A $\beta$  channels based on the solid-state NMR-based  $\beta$  strands, and they found that the ion-permeable A $\beta$  channels are consistent with the results from electron microscopy [28]. Mustata et al. found that small peptide fragments could combine to form an ionic channel [29]. These theoretical works greatly enhanced our understanding of the property of the A $\beta$  ionic channel. However, all these works used the designed A $\beta$  ionic channel as the initial structure to study the shape and ion permeation of the ionic channel. The dynamics and mechanism of A $\beta$  ionic channel formation on the fluidic membrane are still unclear. Understanding the formation process of the A $\beta$  ionic channel on the membrane is very important. It represents not only a fundamental area for academic research, but also gives us an enormous opportunity to improve the quality of life of AD patients. All-atomic (AA) simulation could provide the atomic details and dynamics of the aggregation process of the molecules; however, the timescale is limited up to hundreds of nanoseconds for a large system. Based on Zhou's work [30], coarse grained (CG) MD simulation combined with the MARTINI V2.1 force field could model A $\beta$  core peptides well, and it is widely used and validated as an effective model for studying the assembly of short peptides [31–33]. To better understand the A $\beta$  channel formation process, CGMD simulation was used to perform the system with 25 A $\beta$ 1-28 peptides on the membrane. To make up for the shortcomings of insufficient atomic detail in CGMD, the combination of AA and CG was used to explore the formation process of the A $\beta$  ionic channel. The combined AA and CG method has been successfully used to explore peptide aggregation and pore formation by alamethicin peptides in a hydrated lipid bilayer [34]. Our simulation showed that the ionic channel formed by A $\beta$ 1-28 peptides on the fluid lipid bilayer membrane has a good water permeability.

## 2. Computational Details

### 2.1. Coarse Grained Simulation

The soluble A $\beta$ 1-28 peptide (PDB ID: 1AMB) [35], defined as A $\beta$  peptide, was equilibrated for 10 ns in a water box. The equilibrated A $\beta$  peptides were then transferred into a CG model based on the MARTINI V2.1 force field [36]. After that, 25 A $\beta$  peptides, with the distance of center of mass (COM) between each other of 4.0 nm, were produced in the  $x$ - $y$  plane. All CG A $\beta$  peptides were inserted into a 1,2-dipalmitoyl-sn-glycero-3-phosphocholine (DPPC) membrane, and water molecules were placed in both sides of the membrane. The system consists of 25 A $\beta$  peptides, 1000 DPPC lipids and 20705 water beads in a box of 20 nm  $\times$  20 nm  $\times$  11.0 nm. The parameters of A $\beta$  peptides, DPPC lipids and water beads were extracted as described in MARTINI V2.1 force field. One bead represents the main chain of one residue in A $\beta$  peptides, the benzene ring of phenylalanine is represented by three beads and one water bead represents four water molecules. To investigate the effect of the lipid membranes on the formation process of the ionic channel, another system including 1-palmitoyl-2-oleoyl-sn-glycero-3-phosphocholine (POPC) lipids was also constructed. Two systems, named as AMB-DPPC and AMB-POPC, were equilibrated to 100 ns equilibration by GROMACS 4.6.5 software [37]. Then, all simulations were performed for 5  $\mu$ s with the time step of 20 fs.  $NpT$  ensembles were used with the constant pressures of 1 atm and constant temperature of 310 K. The cutoff for the non-bonded van der Waals interaction was set at 1.2 nm.

### 2.2. All-Atom Molecular Dynamics in an Explicit Solvent

After 5  $\mu$ s CG simulation, the system, including 25 A $\beta$  peptides, DPPC lipids and water beads, was transferred into the AA model with a CHARMM 36 force field [38] by back-mapping tool [39]. The whole system included ca. 420,000 atoms in the AA model. The GROMACS 4.6.5 software was used to perform the simulation. All atoms, including hydrogen atoms, were represented explicitly with the time step of 2 fs, and the length of bonds between hydrogen atoms and other atoms was constrained using SHAKE algorithm [40]. The cutoff for the non-bonded van der Waals interaction was set by a switching function starting at 1.0 nm and reaching zero at 1.2 nm. In all MD simulations,

the particle mesh Ewald (PME) summation [41] was used to calculate the long-ranged electrostatic interactions with periodic boundary conditions (PBC), with a cutoff distance of 1.2 nm for the separation of the direct and reciprocal space. All MD simulations were carried out in NpT ensemble with the constant pressures of 1 atm and constant temperature of 310 K, respectively.

### 3. Results and Discussion

The combination of CG and AA simulations allowed for a complete description of peptides and the pore formation. In the CG simulation process, the pore formation from the A $\beta$  peptides' aggregation was observed. In addition, the transition process from the fibril-type aggregation to pore formation was observed in CG simulation. The AA simulation shows penetration of water molecules and ions into the lipid bilayer through the ionic pore formed by A $\beta$  peptides. The results are discussed in detail in the following subsections.

#### 3.1. Spontaneously Aggregation of A $\beta$ Peptides

All the A $\beta$  peptides remain in the membrane-bound state in the DPPC membrane and laterally diffuse to assemble in aggregates that slowly grow in size. The number of clusters of peptides was measured, with the condition that the two peptides belonged to the same cluster if the distance between the COM of these two peptides was less than 1.5 nm. The evolution of the number of peptide clusters as a function of simulation time is shown in Figure 1. The number of clusters rapidly decreased to 6 in less than 200 ns CG simulation. This shows us that the A $\beta$  peptides tend to aggregate into clusters on the membrane. After a 500 ns simulation, the number of clusters remained at 4 until the end of the 5  $\mu$ s simulation. The simulation was repeated three times, and the number of clusters remained at three and three in the other two trajectories. To explain the aggregation process more clearly, as seen in Figure 2, the snapshots of peptide clusters were captured during the simulation of AMB-DPPC system. Water molecules and DPPC lipids were not presented in the snapshot for clarity. At time = 100 ns, the A $\beta$  peptides had aggregated into eight clusters. Therein, the largest cluster had six A $\beta$  peptides, and all of them had fiber-like parallel aggregation. This shows us that the A $\beta$  peptides are prone to aggregate into fiber even in the membrane. After that, at time = 400 ns, 25 A $\beta$  peptides had aggregated into 4 clusters. The biggest cluster had seven A $\beta$  peptides; the shape of this cluster had changed from the fiber-like to pore-like arrangement, and the other three clusters were not pore shaped. At 4000 ns, the number of cluster was still four, and the number of pore shaped clusters increased to three. As seen in Figure 2D, three clusters aggregated by A $\beta$  peptides were pore shaped. This shows us that the A $\beta$  peptides tend to form the pore shape in the DPPC membrane. To investigate the aggregation process more deeply, the solvent-accessible surface area (SASA) of A $\beta$  peptides in the DPPC membrane was calculated. The correlations between A $\beta$  peptides and the DPPC membrane is provided by examining SASA and the radius of gyration (Rg) of A $\beta$  peptides [42]. The free energy landscape is determined by calculating the normalized probability from a possibility distribution of SASA and Rg, as seen in Equations (1) and (2) [43], where X and Y represent the SASA and Rg.

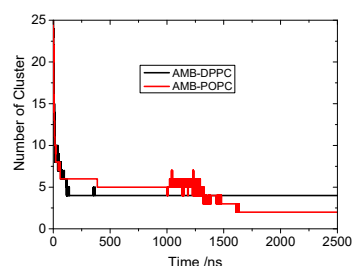


**Figure 1.** The number of peptide (AMB) clusters as a function of simulation time in different membrane systems: DPPC (black line) and POPC (red line).

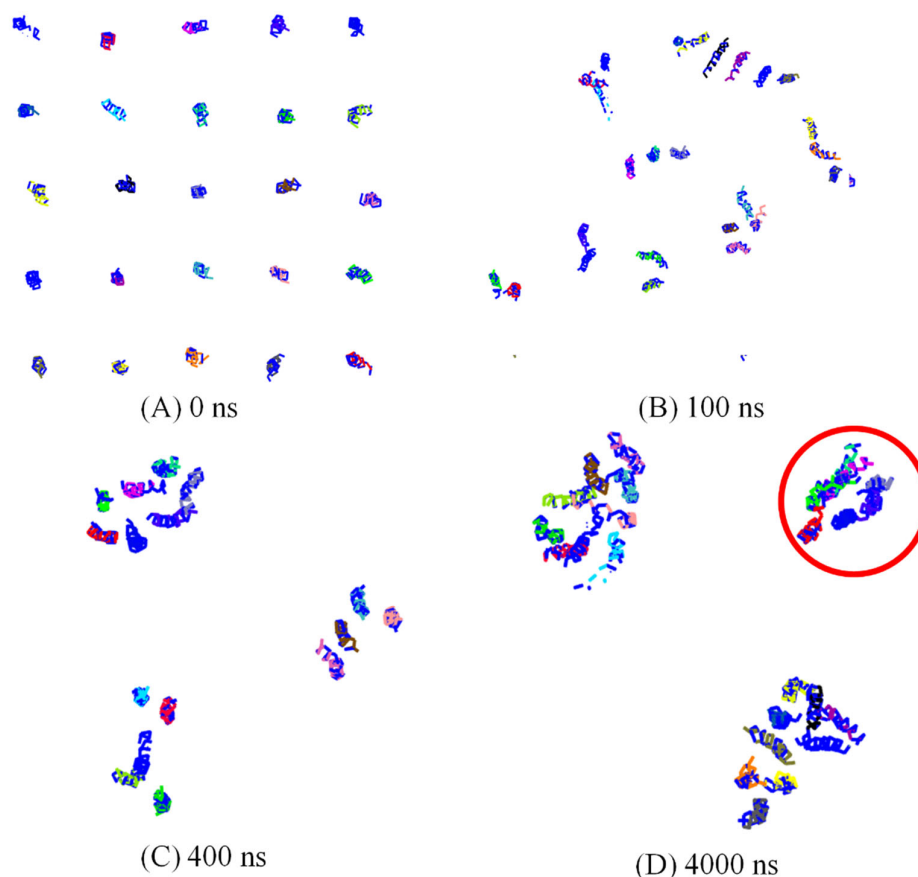


**Figure 2.** The snapshots of peptides clusters were captured in the simulation of the AMB–DPPC system along simulation time: (A) 0 ns; (B) 100 ns; (C) 400 ns and (D) 4000 ns. Water molecules and DPPC lipids were not presented in the snapshot for clarity.

$$P(X, Y) = \frac{1}{Z} \exp[-\beta W(X, Y)] \quad (1)$$

$$\Delta G = W(X_2, Y_2) - W(X_1, Y_1) = -RT \log \left[ \frac{P(X_2, Y_2)}{P(X_1, Y_1)} \right] \quad (2)$$

As shown in Figure 3, the free energy contour maps with two reaction coordinations, SASA and  $R_g$ , are measured. Two important structures could be exacted from the local minimum. One stable structure is the fiber-like structure, and the most stable one is the pore-shaped structure. As mentioned in Yu’s paper [42], the change in structure is accompanied by the change in SASA and  $R_g$ . It could greatly alter the free energy with the change in enthalpy and entropy, and the A $\beta$  peptides could aggregate into a pore-shaped structure or fiber-like structure as seen in Figure S1 (see Supplementary Materials Information). The value of SASA and  $R_g$  is 427.0 nm<sup>2</sup> and 3.60 nm for the pore-like structure, respectively, and it is 428.0 nm<sup>2</sup> and 4.12 nm for the fiber-like structure, respectively. This shows that the value of SASA for these two structures is almost the same. The energy barrier between these two structures is ca. 2.5 kcal/mol from the fiber-like structure to the pore-shaped structure, and it is ca. 3.7 kcal/mol from the pore-shaped structure state to the fiber-like structure state. Although the pore-shaped structure for aggregation of A $\beta$  peptides is much more stable, the energy barrier between these two structures is not very high. This shows us that the conformation of aggregated A $\beta$  peptides from a pore-shaped structure and a fiber-like structure is not very difficult.

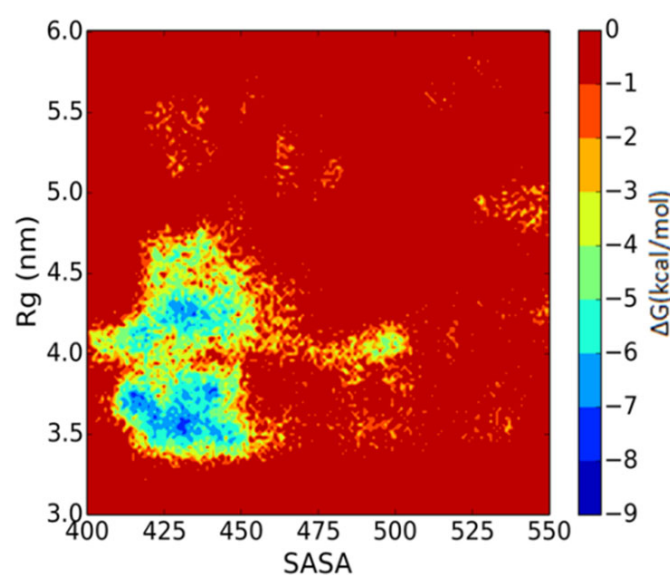


**Figure 3.** Free energy maps vs. two reaction coordinates, the Rg and SASA.

### 3.2. Effect of Lipid Membrane

To investigate the effect of the lipid membrane on A $\beta$  peptides' aggregation, the POPC membrane was used to replace the DPPC membrane in the A $\beta$  peptides aggregation process. In the system including A $\beta$  peptides, DPPC lipids and water molecules, we found only 15 A $\beta$  peptides still remained in the membrane-bound state, and the other 10 A $\beta$  peptides remained in a surface-bound state after the 5  $\mu$ s simulation. As seen in Figure 1, the number of clusters rapidly decreased to 1, and the 15 A $\beta$  peptides remaining in the POPC membrane-spanning state also aggregated into a pore formation structure such as that on the DPPC membrane. This shows us that A $\beta$  peptides tend to aggregate into a pore-like structure in the POPC membrane. Compared with the A $\beta$  peptides' pore-shaped structure on the DPPC structure, the pores formed by A $\beta$  peptides on the POPC membrane are smaller. The shape of the pore formed by A $\beta$  peptides on the POPC membrane is more irregular than that on the DPPC membrane. This implies that it is more difficult for the water molecules and ions to pass through the pore formed on the DPPC membrane than that on the POPC membrane. It shows us that the types of lipid membrane could affect the shape and properties of the pore formed by A $\beta$  peptides. Although 10 A $\beta$  peptides are excluded by POPC membrane, it interacts with the remaining 15 A $\beta$  peptides in the membrane and combines them into one cluster. This also shows us that the interaction between different A $\beta$  peptides' monomers is very strong. In addition, to investigate the shape of A $\beta$  channels more deeply, the order parameter (S) of the largest A $\beta$  peptides' cluster in two systems on different membrane was measured as a function of simulation time. The alpha C atoms of the A $\beta$  channel in the largest cluster were used for the analysis. As shown in Figure 4, the S value of the A $\beta$  channel on two different membranes decreased in the first stage with the aggregation of the A $\beta$  peptides. However, the S value of the A $\beta$  channel on the DPPC membrane is much higher than that of the A $\beta$  channel on the POPC membrane. This means that the arrangement of A $\beta$  peptides in the A $\beta$  channel on the DPPC membrane is more parallel than that on the POPC membrane. It is also the reason why the pore formed by A $\beta$  peptides on the DPPC membrane is larger than that formed by A $\beta$  peptides on the POPC membrane. Due to the membrane fluidity, the S value of the A $\beta$  channels from two systems fluctuated widely in the simulation. It facilitated the conformation change in A $\beta$  peptides during the aggregation process.

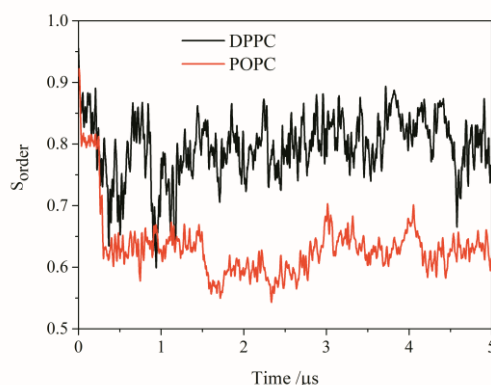


**Figure 4.** The order parameter of the alpha C atoms of the largest A $\beta$  channel as a function of time on a two lipids membrane: POPC and DPPC.

### 3.3. Water Permeation of the Pore

Monitoring the penetration of water molecules into the holes and cavities formed by A $\beta$  peptides' aggregates is a very effective way to assess pore formation in a membrane patch in MD simulations. It is also important to evaluate the toxicity of pores formed by A $\beta$  peptides. The pore formed on the DPPC membrane was selected to investigate the permeation of water molecules. During the CG simulations, only very few water beads interact with the A $\beta$  channel inside the lipid bilayer. In the CG model, one single water bead represents four water molecules, for simplicity. Thus, the total number of water molecules greatly decreases, leading to insufficient visits of water to the channel. Compared to 0.28 nm for an AA water molecule, the vdW diameter of a single water molecule bead is 0.5 nm, which is much larger than the water molecules in the AA model. It is much more difficult for the water bead to enter into the A $\beta$  channel in the membrane. The AA simulation was performed by 100 ns to explore the permeation details of the A $\beta$  channels. The initial structure of the AA model is back mapped from the last structure in the CG simulation, as in our precious work [44].

As shown in Figure 5A, the water molecules could not interact with the inner residue of the A $\beta$  channel in the initial structure. In the AA simulation, the pore was much better established. After performing the 25 ns AA simulation, water molecules could pass through the A $\beta$  channels, as shown in Figure 5B. After that, the conformation of the A $\beta$  channels changes a little in the remainder of the simulation. This shows us that the A $\beta$  channel is very stable on the DPPC membrane, and it confirmed the mechanism of the A $\beta$  channel's formation on the membrane. Limited by the simulation time, the pore of the A $\beta$  channel from the top view is not so cyclical; the radius is estimated ca. 0.55 nm based on the area of the pore. In Nussinov's simulation, the diameter of the A $\beta$  channel is from 0.6 nm to 3.7 nm, from 12 mer to 36 mer peptides [28]. Since the channel is aggregated by seven A $\beta$  peptides in our simulation, the pore size is a little smaller than that from Nussinov's simulation. To investigate the A $\beta$  channel in depth, the passage and distribution of water molecules in the channel were analyzed. Most of water molecules in the A $\beta$  channels could interact with the residues of the A $\beta$  channels directly (the distance between water oxygen atoms and the atom of the peptide is less than 0.4 nm), and the remaining water molecules participated in the water networks to assist with the peptide–water interaction. The water molecule diffusion in A $\beta$  channels is very slow in the initial state, and it is much faster after the expansion of A $\beta$  channels after 25 ns. The density of water molecules and Na<sup>+</sup> ions in the A $\beta$  channels along the z axis was calculated; therein, the z axis of the A $\beta$  channel is from 2.32 nm to 6.55 nm. From the data in Figure 6, the density of water molecules in the A $\beta$  channel is really low compared with that of the bulk. The density of Na<sup>+</sup> ion near the tail of membrane is really high due to the negative charge of the phosphate group. On

the basis of the density of water molecules and  $\text{Na}^+$  ions along the  $z$  axis of the pore, the potential of mean force (PMF) was estimated as follows:

$$\Delta G_{PMF} = -k_B T \ln(\rho_z / \rho_{bulk})$$

Herein,  $k_b$  is the Boltzmann constant,  $T$  is the simulation temperature,  $\rho_z$  is the density of water or  $\text{Na}^+$  in the  $z$  axis of pore and  $\rho_{bulk}$  is the density of water or  $\text{Na}^+$  in the bulk region. An accurate equilibrium PMF relevant to ion permeation should be obtained from the free energy calculations with the umbrella sampling method. However, the ion-density-based PMF could still provide us with the rough relative free energy changes for solvents. The energy barrier for the water molecule to pass through the A $\beta$  channel is ca. 2.51 kcal/mol, and it is 2.02 kcal/mol for the  $\text{Na}^+$  ion. This is a very low energy barrier for the water molecule and  $\text{Na}^+$  ion to pass through the A $\beta$  channel.

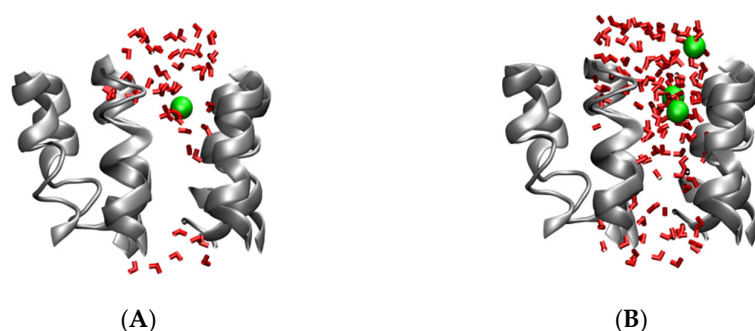


**Figure 5.** (A) is the initial state of the all atomic simulations from a side view; (B) the state after 100 ns, all atomic simulations in side view. The water molecules within 0.8 nm of the channel are shown as a red bonds model,  $\text{Na}^+$  ions within 0.8 nm of the channel are shown in a green CPK model and the A $\beta$  channel is shown by cartoon model in VMD.

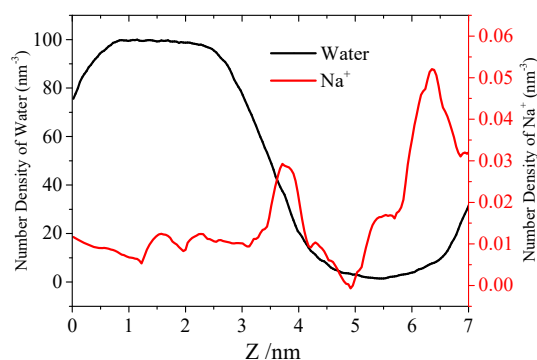


**Figure 6.** The density of water molecules (black line) and  $\text{Na}^+$  ions (red line) along the  $z$  axis of the DPPC membrane.

#### 4. Conclusions

In summary, the pore formation mechanism of A $\beta$  peptides on the membrane and the pore permeation were investigated by combined CG and AA simulation. In the CG simulation, pore-like and fiber-like structures in the aggregation of A $\beta$  peptides on the membrane were observed. The free energy landscape was measured as a function of the change in Rg and SASA, and the pore-like structure is more stable than the fiber-like structure on the membrane. The aggregates do not consist of a specific number of peptides on the membrane, but rather they grow in size over time. In addition, the membrane lipid composition also has an effect on the aggregation process of A $\beta$  peptides. Herein, the pore formation of A $\beta$  peptides on the membrane was observed, and water permeation of the A $\beta$  channel was investigated by AA simulation. Our results demonstrate that the A $\beta$  channel formed by A $\beta$  peptides on the DPPC membrane could have good water permeation.

**Supplementary Materials:** The following supporting information can be downloaded at: <https://www.mdpi.com/article/10.3390/molecules27123924/s1>, Figure S1. The structure of A $\beta$  peptides aggregation: (A) fiber-like formation and (B) pore-like formation.

**Author Contributions:** Conceptualization, Y.D. and L.L.; methodology, Y.D. and Z.X.; software, Y.D. and Z.X.; validation, Y.D., Z.X. and L.L.; investigation, Y.D. and L.L.; resources, Y.D.; data curation, Y.D.; writing—original draft preparation, Y.D. and L.L.; writing—review and editing, Y.D., Z.X. and L.L.; visualization, Y.D.; supervision, L.L.; project administration, L.L.; funding acquisition, L.L. All authors have read and agreed to the published version of the manuscript.

**Funding:** Natural Science Foundation of Zhejiang Province (Grant No. LY21B060004).

**Institutional Review Board Statement:** No applicable.

**Informed Consent Statement:** Not applicable.

**Data Availability Statement:** Not applicable.

**Conflicts of Interest:** There are no conflicts of interest to declare.

## References

1. Strittmatter, W.J.; Roses, A.D. Apolipoprotein E and Alzheimer's disease. *Annu. Rev. Neurosci.* **1996**, *19*, 53–77. [[CrossRef](#)] [[PubMed](#)]
2. Lu, B.; Nagappan, G.; Guan, X.; Nathan, P.J.; Wren, P. BDNF-based synaptic repair as a disease-modifying strategy for neurodegenerative diseases. *Nat. Rev. Neurosci.* **2013**, *14*, 401–416. [[CrossRef](#)] [[PubMed](#)]
3. Heppner, F.L.; Ransohoff, R.M.; Becher, B. Immune attack: The role of inflammation in Alzheimer disease. *Nat. Rev. Neurosci.* **2015**, *16*, 358–372. [[CrossRef](#)] [[PubMed](#)]
4. Moreno-Gonzalez, I.; Soto, C. Natural animal models of neurodegenerative protein misfolding diseases. *Curr. Pharm. Des.* **2012**, *18*, 1148–1158. [[CrossRef](#)] [[PubMed](#)]
5. Salvadores, N.; Shah Nawaz, M.; Scarpini, E.; Tagliavini, F.; Soto, C. Detection of misfolded A $\beta$  oligomers for sensitive biochemical diagnosis of Alzheimer's disease. *Cell Rep.* **2014**, *7*, 261–268. [[CrossRef](#)] [[PubMed](#)]
6. Xiao, Y.; Ma, B.; McElheny, D.; Parthasarathy, S.; Long, F.; Hoshi, M.; Nussinov, R.; Ishii, Y. A $\beta$  (1–42) fibril structure illuminates self-recognition and replication of amyloid in Alzheimer's disease. *Nat. Struct. Mol. Biol.* **2015**, *22*, 499–505. [[CrossRef](#)]
7. Benilova, I.; Karran, E.; de Strooper, B. The toxic A $\beta$  oligomer and Alzheimer's disease: An emperor in need of clothes. *Nat. Neurosci.* **2012**, *15*, 349–357. [[CrossRef](#)]
8. Laganowsky, A.; Liu, C.; Sawaya, M.R.; Whitelegge, J.P.; Park, J.; Zhao, M.; Pensalfini, A.; Soriaga, A.B.; Landau, M.; Teng, P.K. Atomic view of a toxic amyloid small oligomer. *Science* **2012**, *335*, 1228–1231. [[CrossRef](#)]
9. Stroud, J.C.; Liu, C.; Teng, P.K.; Eisenberg, D.P. Toxic fibrillar oligomers of amyloid- $\beta$  have cross- $\beta$  structure. *Proc. Natl. Acad. Sci. USA* **2012**, *109*, 7717–7722. [[CrossRef](#)]
10. Penke, B.; Mária, S.; Ferenc, B. Oligomerization and conformational change turn monomeric  $\beta$ -amyloid and tau proteins toxic: Their role in Alzheimer's pathogenesis. *Molecules* **2020**, *25*, 1659. [[CrossRef](#)]
11. Kotler, S.A.; Walsh, P.; Brender, J.R.; Ramamoorthy, A. Differences between amyloid- $\beta$  aggregation in solution and on the membrane: Insights into elucidation of the mechanistic details of Alzheimer's disease. *Chem. Soc. Rev.* **2014**, *43*, 6692–6700. [[CrossRef](#)] [[PubMed](#)]
12. Sciacca, M.F.M.; Kotler, S.A.; Brender, J.R.; Chen, J.; Lee, D.-k.; Ramamoorthy, A. Two-step mechanism of membrane disruption by A $\beta$  through membrane fragmentation and pore formation. *Biophys. J.* **2012**, *103*, 702–710. [[CrossRef](#)] [[PubMed](#)]
13. Sciacca, M.F.M.; Milardi, D.; Messina, G.M.L.; Marletta, G.; Brender, J.R.; Ramamoorthy, A.; la Rosa, C. Cations as switches of amyloid-mediated membrane disruption mechanisms: Calcium and IAPP. *Biophys. J.* **2013**, *104*, 173–184. [[CrossRef](#)] [[PubMed](#)]
14. Leong, Y.Q.; Ng, K.Y.; Chye, S.M.; Ling, A.P.K.; Koh, R.Y. Mechanisms of action of amyloid-beta and its precursor protein in neuronal cell death. *Metab. Brain Dis.* **2020**, *35*, 11–30. [[CrossRef](#)]
15. Zaretsky, D.V.; Zaretskaia, M.V.; Molokov, Y.I. Membrane channel hypothesis of lysosomal permeabilization by beta-amyloid. *Neurosci. Lett.* **2022**, *770*, 136338. [[CrossRef](#)]
16. di Scala, C.; Yahi, N.; Flores, A.; Boutemour, S.; Kourdougli, N.; Chahinian, H.; Fantini, J. Comparison of the amyloid pore forming properties of rat and human Alzheimer's beta-amyloid peptide 1–42: Calcium imaging data. *Data Brief* **2016**, *6*, 640–643. [[CrossRef](#)]
17. Roche, J.; Shen, Y.; Lee, J.H.; Ying, J.; Bax, A. Monomeric A $\beta$ <sup>1–40</sup> and A $\beta$ <sup>1–42</sup> Peptides in Solution Adopt Very Similar Ramachandran Map Distributions That Closely Resemble Random Coil. *Biochemistry* **2016**, *55*, 762–775. [[CrossRef](#)]
18. Brookes, D.H.; Head-Gordon, T.J. Experimental inferential structure determination of ensembles for intrinsically disordered proteins. *Am. Chem. Soc.* **2016**, *138*, 4530–4538. [[CrossRef](#)]

19. Hou, L.; Shao, H.; Zhang, Y.; Li, H.; Menon, N.K.; Neuhaus, E.B.; Brewer, J.M.; Byeon, I.-J.L.; Ray, D.G.; Vitek, M.P. Solution NMR studies of the A $\beta$  (1–40) and A $\beta$  (1–42) peptides establish that the Met35 oxidation state affects the mechanism of amyloid formation. *J. Am. Chem. Soc.* **2004**, *126*, 1992–2005. [[CrossRef](#)]
20. Petkova, A.T.; Leapman, R.D.; Guo, Z.; Yau, W.-M.; Mattson, M.P.; Tycko, R. Self-propagating, molecular-level polymorphism in Alzheimer's  $\beta$ -amyloid fibrils. *Science* **2005**, *307*, 262–265. [[CrossRef](#)]
21. Petkova, A.T.; Ishii, Y.; Balbach, J.J.; Antzutkin, O.N.; Leapman, R.D.; Delaglio, F.; Tycko, R.P. A structural model for Alzheimer's  $\beta$ -amyloid fibrils based on experimental constraints from solid state NMR. *Proc. Natl. Acad. Sci. USA* **2002**, *99*, 16742–16747. [[CrossRef](#)] [[PubMed](#)]
22. Ciudad, S.; Puig, E.; Botzanowski, T.; Meigooni, M.; Arango, A.S.; Do, J.; Maxim, M.; Mariam, B.; Stephane, C.; Giovanni, M.; et al. A $\beta$  (1–42) tetramer and octamer structures reveal edge conductivity pores as a mechanism for membrane damage. *Nat. Commun.* **2020**, *11*, 1–14. [[CrossRef](#)] [[PubMed](#)]
23. Moore, S.J.; Sonar, K.; Bharadwaj, P.; Deplazes, E.; Mancera, R.L. Characterisation of the structure and oligomerisation of islet amyloid polypeptides (IAPP): A review of molecular dynamics simulation studies. *Molecules* **2018**, *23*, 2142. [[CrossRef](#)] [[PubMed](#)]
24. Itoh, S.G.; Okumura, H. All-atom molecular dynamics simulation methods for the aggregation of protein and peptides: Replica exchange/permutation and nonequilibrium simulations. *Comput. Simul. Aggreg. Proteins Peptides* **2022**, 197–220.
25. Strodel, B. Amyloid aggregation simulations: Challenges, advances and perspectives. *Curr. Opin. Struc. Biol.* **2021**, *67*, 145–152. [[CrossRef](#)]
26. Rezaei-Ghaleh, N.; Amininasab, M.; Kumar, S.; Walter, J.; Zweckstetter, M. Phosphorylation modifies the molecular stability of  $\beta$ -amyloid deposits. *Nat. Commun.* **2016**, *7*, 111359. [[CrossRef](#)]
27. Berhanu, W.M.; Alred, E.J.; Bernhardt, N.A.; Hansmann, U.H.E. All-atom simulation of amyloid aggregates. *Phys. Proc.* **2015**, *68*, 61–68. [[CrossRef](#)]
28. Jang, H.; Arce, F.T.; Capone, R.; Ramachandran, S.; Lal, R.; Nussinov, R. Misfolded amyloid ion channels present mobile  $\beta$ -sheet subunits in contrast to conventional ion channels. *Biophys. J.* **2009**, *97*, 3029–3037. [[CrossRef](#)]
29. Mustata, M.; Capone, R.; Jang, H.; Arce, F.T.; Ramachandran, S.; Lal, R.; Nussinov, R. K3 Fragment of Amyloidogenic  $\beta$ 2-Microglobulin Forms Ion Channels: Implication for Dialysis Related Amyloidosis. *J. Am. Chem. Soc.* **2009**, *131*, 14938–14945. [[CrossRef](#)] [[PubMed](#)]
30. Guo, C.; Luo, Y.; Zhou, R.; Wei, G. Probing the self-assembly mechanism of diphenylalanine-based peptide nanovesicles and nanotubes. *ACS Nano* **2012**, *6*, 3907–3918. [[CrossRef](#)]
31. Bond, P.J.; Holyoake, J.; Ivetac, A.; Khalid, S.; Sansom, M.S.P. Coarse-grained molecular dynamics simulations of membrane proteins and peptides. *J. Struc. Biol.* **2007**, *157*, 593–605. [[CrossRef](#)] [[PubMed](#)]
32. Tsanai, M.; Frederix, P.W.J.M.; Schroer, C.F.; Souza, P.C.; Marrink, S.J. Coacervate formation studied by explicit solvent coarse-grain molecular dynamics with the Martini model. *Chem. Sci.* **2021**, *12*, 8521–8530. [[CrossRef](#)] [[PubMed](#)]
33. Zhao, M.; Sampath, J.; Alamdari, S.; Shen, G.; Chen, C.L.; Mundy, C.J.; Pfandtner, J.; Ferguson, A.L. MARTINI-compatible coarse-grained model for the mesoscale simulation of peptoids. *J. Phys. Chem. B* **2020**, *124*, 7745–7764. [[CrossRef](#)] [[PubMed](#)]
34. Thøgersen, L.; Schiøtt, B.; Vosegaard, T.; Nielsen, N.C.; Tajkhorshid, E. Peptide aggregation and pore formation in a lipid bilayer: A combined coarse-grained and all atom molecular dynamics study. *Biophys. J.* **2008**, *95*, 4337–4347. [[CrossRef](#)] [[PubMed](#)]
35. Talafous, J.; Marcinowski, K.J.; Klopman, G.; Zagorski, M.G. Solution Structure of Residues 1-28 of the Amyloid. beta.-Peptide. *Biochemistry* **1994**, *33*, 7788–7796. [[CrossRef](#)]
36. Monticelli, L.; Kandasamy, S.K.; Periole, X.; Larson, R.G.; Tieleman, D.P.; Marrink, S.-J. The MARTINI coarse-grained force field: Extension to proteins. *J. Chem. Theory Comput.* **2008**, *4*, 819–834. [[CrossRef](#)] [[PubMed](#)]
37. Hess, B.; Kutzner, C.; van der Spoel, D.; Lindahl, E. GROMACS 4: Algorithms for highly efficient, load-balanced, and scalable molecular simulation. *J. Chem. Theory Comput.* **2008**, *4*, 435–447. [[CrossRef](#)]
38. Klauda, J.B.; Venable, R.M.; Freites, J.A.; O'Connor, J.W.; Tobias, D.J.; Mondragon-Ramirez, C.; Vorobyov, I.; Jr, A.D.M.; Pastor, R.W. Update of the CHARMM all-atom additive force field for lipids: Validation on six lipid types. *J. Phys. Chem. B* **2010**, *114*, 7830–7843. [[CrossRef](#)]
39. Wassenaar, T.A.; Pluhackova, K.; Böckmann, R.A.; Marrink, S.J.; Tieleman, D.P. Going backward: A flexible geometric approach to reverse transformation from coarse grained to atomistic models. *J. Chem. Theory Comput.* **2014**, *10*, 676–690. [[CrossRef](#)] [[PubMed](#)]
40. Andersen, H.C. Rattle: A “velocity” version of the shake algorithm for molecular dynamics calculations. *J. Comput. Phys.* **1983**, *52*, 24–34. [[CrossRef](#)]
41. Darden, T.; York, D.; Pedersen, L.J. Particle mesh Ewald: An N $\cdot$ log(N) method for Ewald sums in large systems. *Chem. Phys.* **1993**, *98*, 10089–10092. [[CrossRef](#)]
42. Yu, T.; Schatz, G.C. Free Energy Profile and Mechanism of Self-Assembly of Peptide Amphiphiles Based on a Collective Assembly Coordinate. *J. Phys. Chem. B* **2013**, *117*, 9004–9013. [[CrossRef](#)] [[PubMed](#)]
43. Zhou, R. Trp-cage: Folding free energy landscape in explicit water. *Proc. Natl. Acad. Sci. USA* **2003**, *100*, 13280–13285. [[CrossRef](#)] [[PubMed](#)]
44. Liang, L.; Wang, L.W.; Shen, J.W. The self-assembly mechanism of tetra-peptides from the motif of  $\beta$ -amyloid peptides: A combined coarse-grained and all-atom molecular dynamics simulation. *RSC Adv.* **2016**, *6*, 100072–100078. [[CrossRef](#)]